Field-free all-optical switching and electrical readout of Tb/Co-based magnetic tunnel junctions

D. Salomoni, Y. Peng, L. Farcis, S. Auffret, Michel Hehn, Grégory Malinowski, Stéphane Mangin, B. Dieny, L. D. Buda-Prejbeanu, Ricardo C. Sousa, et al.

▶ **To cite this version:**

D. Salomoni, Y. Peng, L. Farcis, S. Auffret, Michel Hehn, et al.. Field-free all-optical switching and electrical readout of Tb/Co-based magnetic tunnel junctions. Physical Review Applied, 2023, 20 (3), pp.034070. 10.1103/PhysRevApplied.20.034070 . hal-04227118

HAL Id: hal-04227118
https://hal.science/hal-04227118

Submitted on 3 Oct 2023

HAL is a multi-disciplinary open access archive for the deposit and dissemination of scientific research documents, whether they are published or not. The documents may come from teaching and research institutions in France or abroad, or from public or private research centers.

L'archive ouverte pluridisciplinaire **HAL**, est destinée au dépôt et à la diffusion de documents scientifiques de niveau recherche, publiés ou non, émanant des établissements d'enseignement et de recherche français ou étrangers, des laboratoires publics ou privés.

Field-free all-optical switching and electrical read-out of Tb/Co-based magnetic tunnel junctions

D. Salomoni,* L. Farcis, S. Auffret, B. Dieny, L. D. Buda-Prejbeanu, R.C. Sousa, and I. L. Prejbeanu†
Univ Grenoble Alpes, CEA, CNRS, Grenoble INP, SPINTEC, 38000 Grenoble, France.

Y. Peng, M. Hehn, G. Malinowski, and S. Mangin
Institut Jean Lamour, UMR CNRS 7198, Université de Lorraine, 54011 Nancy, France
(Dated: October 3, 2023)

Switching of magnetic tunnel junction using femtosecond laser pulses enables a possible path for non-volatile, ultrafast and low-dissipative memories. In this work we demonstrate successful field-free 50 fs single laser pulse driven magnetization reversal of [Tb/Co] based storage layer in a perpendicular magnetic tunnel junction with a record estimated absorbed energy of 68.6 fJ/bit. The nanofabricated magnetic tunnel junction devices have an optimized bottom reference electrode and show tunnel magnetoresistance ratio values (TMR) up to 74% after patterning down to sub-100 nm lateral dimensions. Experiments on continuous films reveal peculiar reversal patterns of concentric rings with opposite magnetic directions, above certain threshold fluence. These rings have been correlated to patterned device switching probability as a function of the applied laser fluence. Moreover, the magnetization reversal is independent of the duration of the laser pulse. According to our macrospin model, the underlying magnetization reversal mechanism can be attributed to an in-plane reorientation of the magnetization due to a fast reduction of the out-of-plane uniaxial anisotropy and a magnetization precession around the local effective anisotropy axis. These aspects are of great interest both for the physical understanding of the switching phenomenon and their consequences for all-optical-switching memory devices, since they allow for a large fluence operation window with high resilience to pulse length variability.

I. INTRODUCTION:

Conventional computer memories have evolved into a many-level hierarchy where the operation speed, storage density and cost, define a trade-off leading to the implementation of different memory technologies. As the physical limits of complementary metal oxide semiconductor (CMOS) memories are reached, the possibility to replace volatile memory with fast non-volatile alternatives has been a compelling argument of Magnetoresistive Random Access Memory (MRAM)[1–3]. Perpendicular spin transfer torque (STT) MRAM, due to advantages such as reliable switching, low energy consumption and easy integration with CMOS technology [1], is the most widely foundry adopted spintronics based memory [4–6]. High-performance STT magnetic tunnel junction (MTJ) cells are among the first MRAMs to have recently been commercialized as embedded flash memory and last-level cache replacements. The FeCoB/MgO/FeCoB system has become the basis of most MTJ designs, due to its high tunnel magnetoresistance ratio effect (TMR) [7, 8], improved readability and scaling of interfacial perpendicular magnetic anisotropy (PMA) [9, 10] based devices. Moreover, in STT cells the reading and writing paths are shared enabling a compact design [11, 12], however fast switching in the precessional regime requires switching voltages close to the barrier breakdown voltage.

Alternative Spin-Orbit Torque (SOT) technology, is more suitable for high-speed and low error rate operation [13, 14]. The SOT three terminal devices with separate reading and writing paths enable better endurance combined with fast switching, creating a potential replacement for static random-access memories (SRAM) [15]. Its main drawback is the larger bit-cell area, and although switching pulses as short as 100 ps are possible, the application of a field is generally required to obtain deterministic switching which complexifies the cell design.

The all-optical-switching (AOS) technology envisions to further accelerate the magnetization reversal process by enabling writing the cells at femtosecond time scales. Single Pulse All Optical Helicity Independent Switching (AO-HIS) is a phenomenon by which the magnetization of a nanostructure can be reversed by a single femtosecond laser pulse. The method is ultrafast and does not require use of any applied field. Since its discovery in GdFeCo ferrimagnetic systems [16], single pulse AO-HIS had been limited to Gd-based alloys or Gd/FM bilayers, where FM is a ferromagnetic layer [17, 18]. Only recently few other material systems have shown switching driven by ultrashort laser pulses: MnRuGa ferrimagnetic Heusler alloys [19], Tb/Co multilayers [20–22], Tb/Fe and $Tb_{32}Co_{68}$/Co trilayer[23]. An encouraging spin valve alternative mechanism has been recently explored in [24] where angular momentum is brought from one layer to the other one allowing rare-earth free switching. As demonstrated in this paper, AO-HIS mechanism for Tb based heterostructures is very different than the one observed for Gd based materials.

Using AOS as a write mechanism in MRAM is ex-

* david.salomoni@cea.fr
† ioan-lucian.prejbeanu@cea.fr

pected to enable writing at speeds 2 orders of magnitude faster than electrical alternatives with an energy as low as 16 fJ/bit [3], while maintaining non-volatility [3, 19]. This, not only increases speed and reduces power consumption, but also allows for more compact two terminal design of STT devices, with no compromise in endurance.

The first successful AOS operation of a micron-sized p-MTJ cell was demonstrated by Chen et al [25], using a GdFeCo alloy storage layer, leading to a small TMR ratio of 0.6%. It was later improved by Wang et al.[26], who reported switching of Co/Gd bilayer tunnel junctions with cell sizes down to 3 µm lateral size and TMR ratio of 34.7%. The increase of TMR was possible thanks to a clever design demonstrated by Avilés-Félix et al.[20, 21, 27] where to enable AOS in a MTJ the optically-switchable material is coupled magnetically to the FeCoB interface of the storage layer. The initial reports of a storage layer based on $[Tb/Co]_N$ multilayer coupled to a FeCoB showed the possibility to adjust the Co/Tb composition in order to control the effective perpendicular anisotropy of magnetic tunnel junctions [20, 21]. The perpendicular anisotropy could be maintained without degradation even after annealing at 250° C to obtain 38% TMR after patterning. Thin film experiments of the same storage layer stacks confirmed AO-HIS of the magnetization with both 60 fs and 5 ps laser pulses for incident fluences down to 3.5 mJ/cm^2. However, reliable and field-free AOS demonstration on patterned devices and a clear understanding of the switching mechanism of this system are missing so far.

In this work, we developed MTJ devices comprising a $[Tb/Co]_5$ based top storage layer with diameters from 300 nm down to 80 nm exhibiting TMR values up to 74%. We demonstrate field-free helicity independent all optical toggle switching driven by 50 fs single light pulse on a [Tb/Co] based p-MTJ patterned to sub-100 nm lateral dimensions. The comparison of patterned device properties to those of continuous film, shows that high anisotropy of the Tb/Co based electrode is maintained after patterning. The integration of a stable reference layer, with low offset field, does not degrade the AOS stack properties. Furthermore, the AOS behaviour seen at film level correlates with pattern device switching probability, despite the evident changes in the magnetostatic interaction. The underlying reversal mechanism that takes place in these systems is analyzed in the framework of a macrospin model accounting for the temperature dependence of the anisotropy.

II. RESULTS AND DISCUSSION:

Our samples depicted in Fig. 1a have a bottom synthetic anti-ferromagnetically (SAF) coupled reference layer based [Co/Pt] multilayer, as the one used in conventional STT-MRAM cells. The complete magnetic stack deposited by DC magnetron sputtering is: Ta(3)/Pt(25)/[Co(0.5)/Pt(0.25)]x5/Co(0.5)/Ru(0.9)/ [Co(0.5)/Pt(0.25)]x2/Co(0.5)/W(0.3)/FeCoB(1)/ $MgO(t_{Mg})$/FeCoB(1.4)/W(0.2)/$[Tb(t_{Tb})/Co(t_{Co})]$x5/ W(2)/Pt(5), where all the thicknesses in brackets are expressed in nm. Samples were deposited using Ar pressure of 2 x 10^{-3} mbar, base pressure of 10^{-8} mbar and annealed at 250°C. The samples were deposited using a double-wedge thicknesses for Tb and either MgO or Co to allow for the investigation of devices properties as function of layer thickness, as in [20].

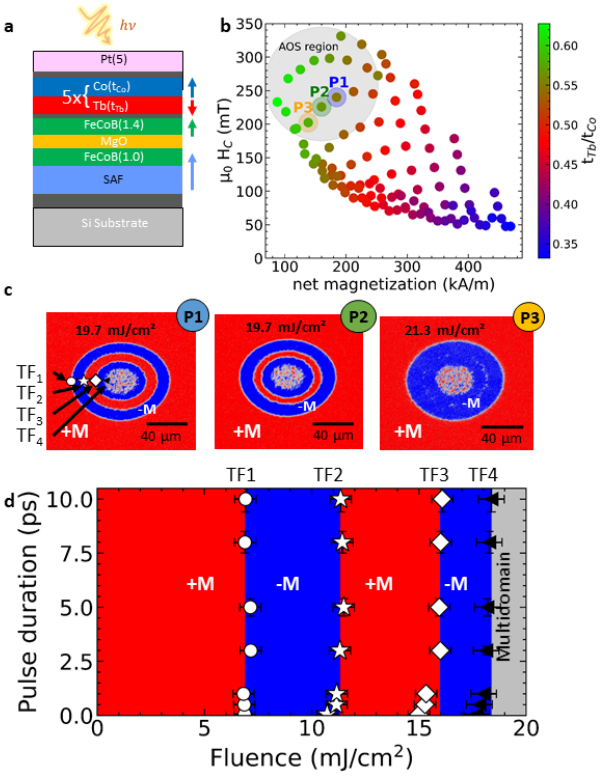

FIG. 1. a) AOS-MTJ stack with bottom-pinned and [Tb/Co]ML storage layer schematic. b) MOKE magnetometer measured coercive field vs net magnetization, $M_{S,\,Co}$ = 760 kA/m, $M_{S,\,Tb}$ = 1350 kA/m [28, 29]. c) Background subtracted MOKE images after single 50 fs laser pulse of different fluences, and for positions: P1 (t_{Co}: 1.37nm,t_{Tb}: 0.76 nm), P2 (t_{Co}: 1.41 nm,t_{Tb}: 0.80 nm) and P3(t_{Co}: 1.45 nm,t_{Tb}: 0.86 nm). d) Pulse duration vs fluence experimental state diagram of the magnetization reversal. Threshold (ring) boundaries: TF1 outer-border red to blue; TF2 blue to red border; TF3 second red to blue border; TF4 center demagnetized multidomain.

The AO-HIS properties of our multilayered samples before nanopatterning were systematically analysed by magneto-optical Kerr effect microscopy (MOKE). The pump laser beam used in the AOS measurement was generated by a Ti:sapphire femtosecond-laser source with a wavelength of 800 nm and a repetition rate of 5 kHz. The Gaussian beam diameter of 100 µm was determined by directly observing the beam at the focal plane of the microscope lens and later confirmed using the reversed domain size as function of the pulse energy. The source

for the background-subtracted MOKE images, depicted in Fig. 1c and Fig. 2b, was an LED light emitting at a wavelength of 628 nm. The measurements were carried out without the requirement for synchronization, as they were conducted under static conditions. The methodology consisted of applying individual laser shots followed by a sample measurement after each pulse. Depending on the substrate material, either a transmission or reflection configuration was employed: transmission for glass substrates and reflection for silicon substrates, with further details available in [23]. Regardless of the configuration, the system shows AOS close to the magnetization compensation region at room temperature and on the Co-rich region where the Co magnetization is dominant, no significant differences were found for the two types of substrates. Similar to previous reported [Tb/Co] multilayers [21] with 5 bilayer repetitions annealed at 250^o C the Tb thickness range is from 0.6 to 0.9 nm, and respectively 1.2 to 1.5 nm for Co. In Fig. 1b it is shown the coercive field vs net magnetization for Tb/Co thickness ratio, with the highlighted region where AOS is occurring (gray area).

The net magnetization was determined based on the thickness of deposited Tb and Co layers, using M_S values from references [28, 29]. We used a MOKE magnetometer for the measurements, enabling us to pinpoint the magnetization compensation point and address possible fluctuations in the deposition rate and disparities from established M_S values in literature sources.

As one can see to have AOS the system needs to be close to the compensation point where M_S is relatively low and anisotropy, that is proportional to the coercive field, is high. In this AOS thickness region a strong reduction of anisotropy and increase of net magnetization with temperature was shown by [22, 23].

After each single laser pulse a complete full signal amplitude toggle reversal of the storage layer occurs. This behavior is reproducible for the storage layer stack up to 150,000 consecutive pulses, suggesting that the toggle switching has a large endurance and repeatability for the above thickness ranges.

For fluences higher than 11 mJ/cm^2, the reversed domains exhibit concentric rings with opposite magnetic directions (as seen in Fig. 1c and Fig. 2b). It is noteworthy that similar behaviour was also observed for samples with only [Tb/Co] multilayers, excluding any contribution from the SAF reference layer to the magnetization reversal, except for its impact as a heat sink structure increasing the fluence threshold of the different regions [23]. From the outside inwards four fluence thresholds (TF1-TF4), for the reversal or non-reversal, were identified taking into account the gaussian profile of the laser spot. Based on the MOKE observation upon varying the laser pulse duration it was possible to draw a complete state diagram of pulse duration versus fluence, as reported in Fig. 1d. The type of reversal, either concentric rings or single domain, is dependent on the multilayer respective thicknesses. As shown in Fig. 1c for positions P1, P2 and P3, the threshold fluences TF2 and TF3 defining the presence of the second ring, having the same magnetization as the initial state (red contrast), are brought closer with increasing Tb and Co thickness, merging together for Tb:0.86 nm / Co:1.45 nm at P3, to form a single reversed domain. This effect can be assigned to an increase in the Gilbert damping due to the increased Tb content [30, 31]. As reported in [23] and contrary to Gd based materials, the fluence required to reverse and stabilize a given number of rings has little or no dependence on the laser pulse duration. Single pulse reversals were obtained for pulse duration from 50 fs up to 12 ps, the maximum pulse duration available on the laser setup.

Recently we have studied the possible origin of these peculiar AOS properties pointing towards an in-plane magnetization reorientation with a precessional switching mechanism. The reported state diagrams observed for Tb/Fe, and $Tb_{32}Co_{68}$/Co trilayer [23] share the same similarities as those of the [Tb/Co] multilayers, proving that a similar magnetization reversal process takes place in these Tb based multilayer systems.

The independence of pulse duration suggests that the reversal mechanism proceeds for a time longer than the laser pulse itself and is slower than the one observed in Gd based samples [17]. Considering a two temperature model, at the short time scale up to a few ps the behaviour of the electron temperature T_e is highly dependent on the laser pulse duration. Within few ps the T_e relaxes to the phonon temperature T_p and, from there on, the time evolution of the two becomes indistinguishable. For longer times, in the order of tens/hundreds of ps, the reached temperatures are only due to the laser fluence and cooling of the system to the thermal bath. Based on the experimental results, we understand that the key dynamics for the reversal occur during the longer time phase. This interpretation is based on the fact that super-diffusive spin currents [32], hot electrons and ultrafast demagnetization [33] are effects highly dependent on pulse duration. This is contrary to our experimental observations where the final reversed state is essentially independent of the laser pulse length up 12 ps and probably beyond. The initial fast response phase certainly plays a role at the beginning of the reversal, and may be more important for fs pulses, but does not determine the end-state.

Hence, we developed a phenomenological macrospin model based on the Landau-Lifshitz-Gilbert equation coupled to two temperature model [34] to assess whether the above assumptions are consistent with the main features of our observations, providing an insight into the underlying reversal process taking place at the ps timescale.

The model accounts for two key features: i) fast drop of the uniaxial anisotropy K_u with temperature and ii) small tilt of the uniaxial anisotropy axis with respect to the out-of-plane direction, chosen to be towards the x axis, $\boldsymbol{u_k} = (\sin\theta_u, 0, \cos\theta_u)$, $\theta_u > 0^o$. The energy density

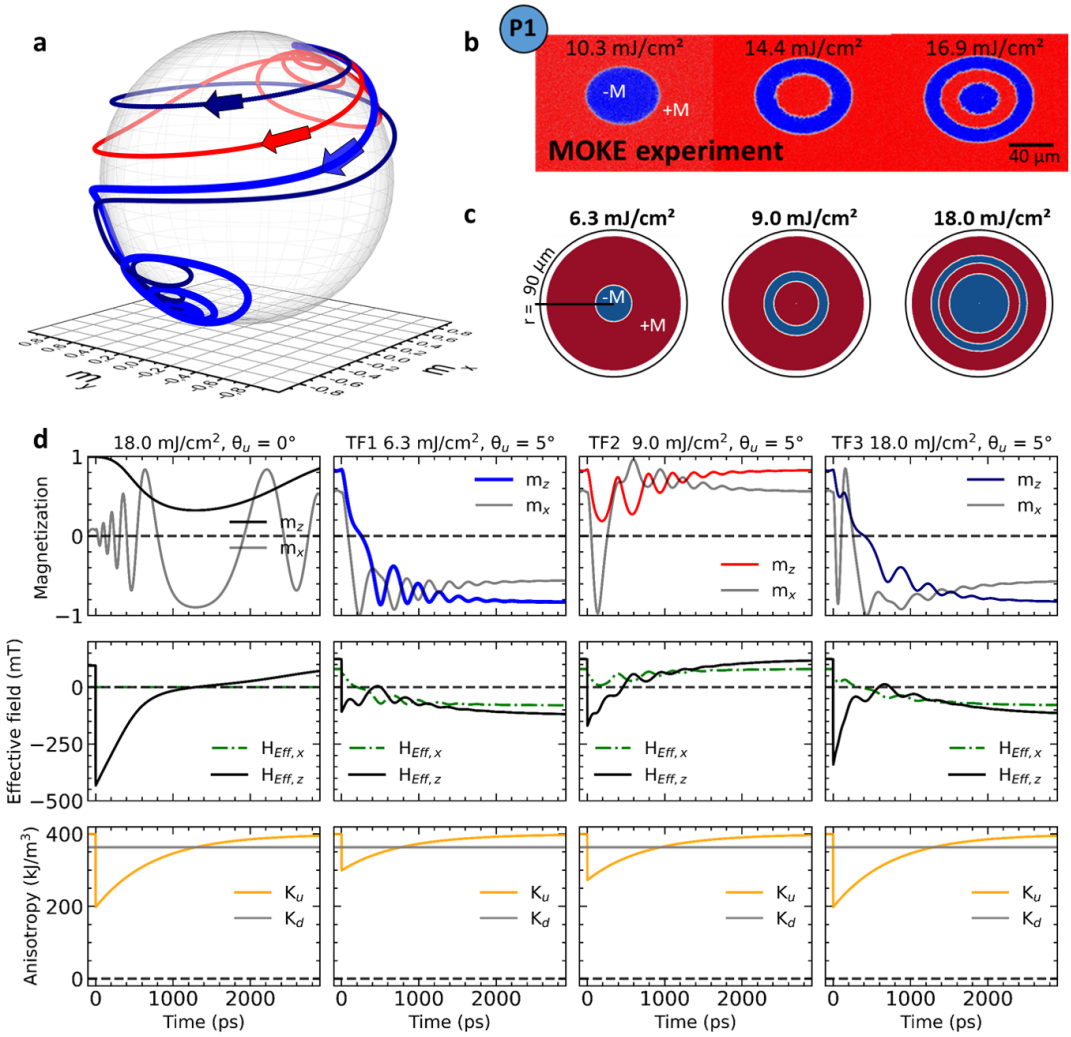

FIG. 2. a) Magnetization dynamics 3D view as predicted by macrospin model. b) For position P1 (Fig. 1b), experimental background subtracted MOKE images, laser: 50 fs and 10.3 mJ/cm^2, 14.4 mJ/cm^2, 16.9 mJ/cm^2. c) Expected magnetization pattern after 100 fs for a single Gaussian shaped laser pulse with spins fully independent. Simulations in a),c) were performed for $\theta_u = 5^o$, $M_s = 760$ kA/m and $K_{u,300K} = 1.1 \cdot \frac{\mu_0 M_s^2}{2}$, Gilbert damping $\alpha = 0.1$. d) m_z, m_z, $H_{eff,\,x}$, $H_{eff,\,z}$ and K_u time traces for $\theta_u = 5^o$ fluences 6.3 mJ/cm^2, 9.0 mJ/cm^2, 18.0 mJ/cm^2, and $\theta_u = 0^o$ fluences 18.0 mJ/cm^2.

of the system, assuming a continuous film approximation, is given by $E_{tot} = -K_u(\boldsymbol{u_k} \cdot \boldsymbol{m})^2 + \frac{1}{2}\mu_0 M_S^2 m_z^2$, where $\boldsymbol{m}$ is unitary vector. The phenomenological relation used for the anisotropy is $K_u(T) = K_{u0}[1 - (\frac{T}{T_C})^{1.73}]^2$, where $T_C = 450$ K is a critical temperature [35]. As a first approximation the simulations were performed assuming constant M_s, and as a consequence constant demagnetizing anisotropy $K_d = \frac{1}{2}\mu_0 M_s^2$. The fact that the Co rich region is expected to increase M_s with temperature [22] is not a concern as this would further promote the in-plane reorientation. This instead is not true for the Tb rich region where the M_s is expected to drop fast with temperature, and no AOS is observed.

In Fig. 2d the calculation for the reversal mechanism is shown for $\theta_u = 5^o$ at increasing fluence (columns 2,3 and 4) and compared to column 1 where no tilt is present. After the laser pulse, the demagnetizing field overcomes the anisotropy, the magnetization starts precessing towards the plane. If $\theta_u = 0^o$ the precession occurs only around the z axis and no crossing of the x,y plane is possible. Instead, the small tilt introduces a x component in the effective field ($\boldsymbol{H_{eff}} = -\frac{1}{\mu_0 M_s}\frac{\delta E_{tot}}{\delta \boldsymbol{m}}$) that strongly affects the trajectory of the magnetization and drives the reversal.

The precession occurs for a time that depends on the energy absorbed, i.e. the laser fluence. The anisotropy field recovers during the precession due to cooling ($K_d < K_u$). As the fluence increases, the number of rotations made by the magnetization during precession increases. Depending whether the number of half-rotations is odd or even, the magnetization will end up as reversed or not reversed resulting in the concentric rings pattern shown

in Fig. 1c and Fig. 2b,c.

Although the model is fairly simple, it is able to correctly predict the main features of our [Tb/Co] multilayer system. The perpendicular anisotropy originating from the Tb/Co interface [36] is known to have an important temperature dependence, with typical blocking temperatures below 200° C due to the low Curie temperature of Tb (237 K for bulk measurements [37]). The assumption of a tilted axis for the anisotropy is supported by the quasi-static measured hysteresis loop in Fig.4c, showing a gradual saturation for higher perpendicular fields, which indicates the existence of an in-plane component. The presence of in-plane uniaxial anisotropy in [Tb/Co] multilayers has already been reported [36], providing further justification to consider it. The origin of a local tilt may be attributed to the sperimagnet nature of Tb [38] or poly-crystalline nature of the Tb/Co multilayer. According to our simulation, to have magnetization reversal, the perfect out-of-plane symmetry has to be broken thus the tilt angle needs to be greater than 0 degrees. We observed that lower the tilt smaller the fluence switching window is. We chose a value of 5 degrees as the fluence required to commute was consistent with the experimental observations. Our additional simulations indicate that equivalent behaviour is found for a tilt angle between 2 to 15 degrees. The fluence threshold would change with the tilt value in this window but the overall behaviour is similar. As shown by the magnetization time traces in Fig.2d, the total time for reversal is expected to be of the order of tens/hundreds of ps, but the final magnetization state is determined by the first few precessions. Currently, our model presents one possible scenario to be confirmed by future work. It offers a strong and coherent grasp of the observed magnetization reversal behaviors, even without factoring in the rapid partial demagnetization caused by the sudden rise in electron temperature. Addressing this requires more detailed atomistic or Landau-Lifshitz-Bloch (LLB) models, which we plan to explore in an upcoming study.

Next, we introduced this Tb/Co based thin films as storage layer in full MTJ stacks with optical access enabling AOS writing and electrical readout. Nanopillars were fabricated on a cross-wedge thickness sample annealed at 250° C, keeping a Co layer thickness fixed at 1.4 nm while varying the Tb layer thickness from 0.4 nm to 1.1 nm across a 100 mm Si(100) wafer, to include the known AOS thickness region for Tb 0.7-0.9 nm. Perpendicularly, a cross-wedge of the MgO barrier was deposited, with thickness ranging from 1.1 nm to 3.0 nm to characterize the optimal Mg natural oxidation thickness to achieve the highest TMR ratio.

The nanofabrication process includes an indium tin oxide (ITO) as transparent conductive electrode to provide an optical access to the top electrode of magnetic tunnel junction (details in [39]). Fabricated MTJ devices with diameters from 300 nm down to 80 nm show no impact on the expected AOS stack properties from the reference layer with typical offset fields below 200 Oe. Indeed, high

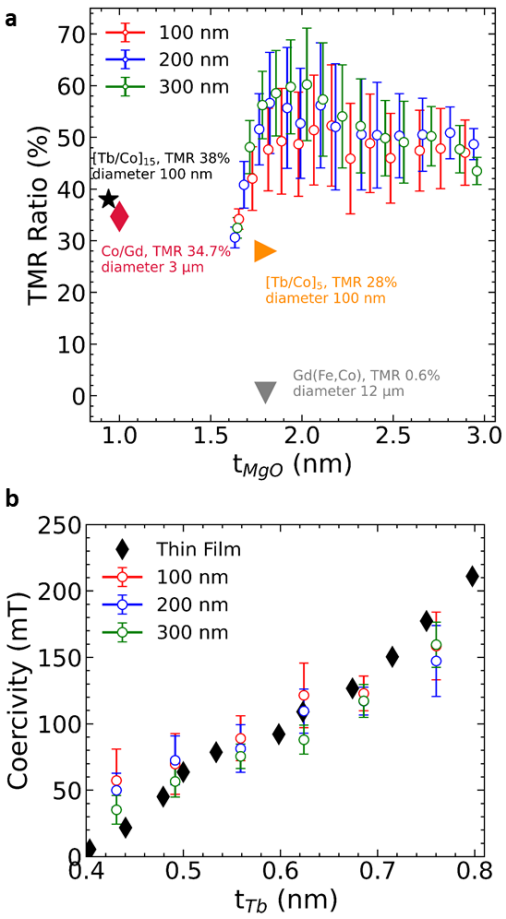

FIG. 3. a) The device average TMR versus naturally oxidized MgO thickness for nominal diameter between 100 nm to 300 nm and thicknesses t_{Tb} from 0.5 nm to 0.75 nm and t_{Co}=1.4 nm, respectively compared to literature values[21, 25, 26, 39]. b) Coercive field vs Tb thickness comparison between thin film sample and nano-patterned devices.

perpendicular anisotropy at film level is maintained after nanopatterning as shown by the patterned and thin film coercivity in Fig. 3b. The coercivity depends on Tb/Co thickness, but stays comparable before and after patterning without substantial dependency on diameter. Device average TMR for each pillar nominal diameters from 80 nm to 300 nm versus naturally oxidized MgO thickness are compared to literature values in Fig. 3a, for a Tb thickness of 0.5 nm. The natural oxidation time was fixed to 2 steps of 10 s at 150 mbar. The optimal Mg thickness is 2 nm, below this value the tunnel barrier is over oxidized leading to lower TMR values. This stable reference layer combined with optimized Mg natural oxidation thickness allows us to get highest TMR values of 74% representing a 2 times improvement compared to the highest AOS-MTJ reported so far[20, 21, 25, 26, 39].

The all-optical switching properties of nanosized MTJ pillars were investigated using linearly polarized fs laser pulses while measuring the resistance of the junction, as

illustrated in the schematics of Fig. 4a. The electrical readout was performed using a digital multimeter connected to the device top and bottom electrodes by wire-bonding. The resistance was measured applying a continuous reading voltage of 10 mV. All measurements were performed without any external magnetic field, without compensating offset fields from the reference layer. Fig. 4d shows an example of a 100 nm AOS-MTJ that can be repeatedly toggled between parallel (P) and anti-parallel (AP) states, showing the full 50% TMR resistance change expected from the R-H loop in Fig. 4c.

The absorbed energy, calculated assuming a 17.5% absorption of the laser fluence (from [40] on a similar stack) multiplied by the area of the pillar, was estimated to be 68.6 fJ/bit. This is already much lower than the dissipation writing energy of existing technologies like hard disk drives (10-100 nJ)[41], FLASH-memory (10 nJ)[42], and to state-of-art STT-RAM (450 pJ-100 fJ)[3, 43], but the corresponding energy for a diameter of 40 nm pillar is 11 fJ/bit, 45% less than the prediction in [3].

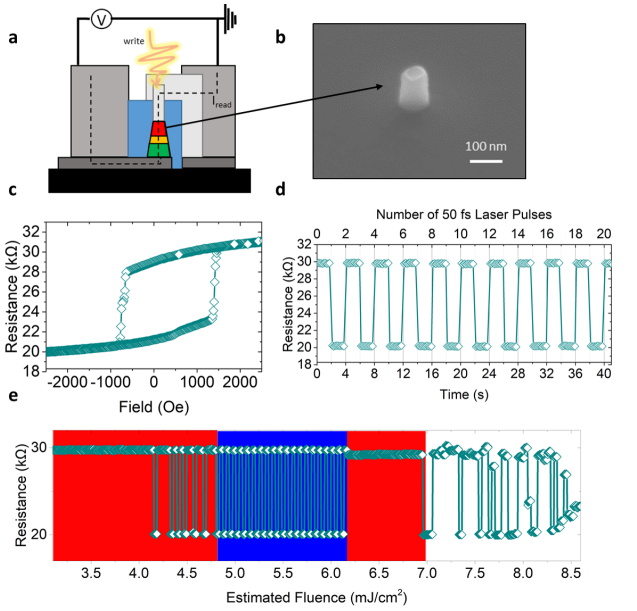

FIG. 4. a) Schematic illustration of all-optical writing and electrical reading of AOS-MTJ. b) SEM image of 100 nm in diameter pillar. c) AOS-MTJ hysteresis R-H loop, field applied out-of-plane. d) TMR measurement as a function of time upon laser-pulse excitation. e) TMR measurement using constant 1 Hz laser frequency and incremental laser power for each pulse.

In Fig. 4e we compare the fluence write levels between the patterned tunnel junction and the equivalent AOS stack at thin film level. The switching dependence on fluence appears to be preserved after patterning. In the performed experiment, the laser was shot repeatedly at a frequency of 1 Hz, while increasing the laser power with a step of 0.01 mW every second. It allows probing the minimum fluence for which a reversal is obtained. At low fluence, there is no switching, and some switching events are observed starting at 4 mJ/cm^2. In a region from 5-6 mJ/cm^2 the switching probability is 100% as highlighted in blue in Fig. 4. For even higher fluence, in the region highlighted in red, switching is no longer observed, followed by random switching before an eventual device degradation. There is a strong correlation between this established device phase diagram and that of the thin film from Fig. 1d), indicative of a very similar reversal mechanism responsible for the alternating of reversal and non-reversal regions. In the framework of our model the same precessional switching reversal process determines the AOS properties of the patterned device, despite the fact that some stray field from the reference layer is acting on the storage layer.

III. CONCLUSION:

In conclusion, we have integrated a bottom reference p-MTJ with an all-optical-switchable $[Tb/Co]_{x5}$ based storage layer, the resulting continuous film and patterned devices having similar magnetic properties. This system shows all-optical-switching for Co-rich regions close to the magnetization compensation region at room temperature for a Tb thickness range of 0.6 nm to 0.9 nm, and Co 1.2 nm to 1.5 nm. We developed a macrospin model able to predict several characteristic features observed experimentally. Thus the magnetization reversal process appears to be driven by an in-plane reorientation of the magnetization coupled to a precessional switching mechanism. The model explains the experimentally observed concentric rings of opposite magnetization directions that appear at high laser fluence. Remarkably, both experiments and simulations indicate that the threshold fluences do not depend on the pulse duration but rather on the AOS layer thicknesses. This represents a significant advantage of the Tb/Co material providing high resilience to pulse length variability at the device level. Furthermore, the implementation of a stable reference layer and optimization of the MgO natural oxidation allowed for TMR values of 74%, the highest reported so far for AOS-MTJs. Field-free helicity independent all optical toggle switching was demonstrated on 100 nm patterned [Tb/Co] p-MTJ devices, driven by 50 fs laser pulses for an absorbed energy of 68.6 fJ/bit. These findings pave the way towards nanoscale devices for optospintronic embedded memories combining non-volatily with ultrafast and energy-efficient writing.

ACKNOWLEDGMENTS

We acknowledge financial support from the ANR (ANR-17-CE24-0007 UFO project) and European Union's Horizon 2020 research and innovation programme under Marie Skłodowska-Curie grant agreement No 861300 (COMRAD), this work is supported by the Institute Carnot ICEEL for the project "CAPMAT" and

FASTNESS, the Région Grand Est, the Metropole Grand Nancy, for the Chaire PLUS by the impact project LUE-N4S, part of the French PIA project "Lorraine Université d'Excellence" reference ANR-15-IDEX-04-LUE, the "FEDERFSE Lorraine et Massif Vosges 2014-2020" for PLUS and IOMA a European Union Program.

[1] B. Dieny, I. L. Prejbeanu, K. Garello, P. Gambardella, P. Freitas, R. Lehndorff, W. Raberg, U. Ebels, S. O. Demokritov, J. Akerman, *et al.*, Opportunities and challenges for spintronics in the microelectronics industry, Nature Electronics **3**, 446 (2020).

[2] J. Kim, A. Paul, P. A. Crowell, S. J. Koester, S. S. Sapatnekar, J.-P. Wang, and C. H. Kim, Spin-based computing: Device concepts, current status, and a case study on a high-performance microprocessor, Proceedings of the IEEE **103**, 106 (2014).

[3] A. V. Kimel and M. Li, Writing magnetic memory with ultrashort light pulses, Nature Reviews Materials **4**, 189 (2019).

[4] J. C. Slonczewski, Current-driven excitation of magnetic multilayers, Journal of Magnetism and Magnetic Materials **159**, L1 (1996).

[5] L. Berger, Emission of spin waves by a magnetic multilayer traversed by a current, Physical Review B **54**, 9353 (1996).

[6] D. C. Ralph and M. D. Stiles, Spin transfer torques, Journal of Magnetism and Magnetic Materials **320**, 1190 (2008).

[7] S. Yuasa, T. Nagahama, A. Fukushima, Y. Suzuki, and K. Ando, Giant room-temperature magnetoresistance in single-crystal fe/mgo/fe magnetic tunnel junctions, Nature materials **3**, 868 (2004).

[8] S. S. Parkin, C. Kaiser, A. Panchula, P. M. Rice, B. Hughes, M. Samant, and S.-H. Yang, Giant tunnelling magnetoresistance at room temperature with mgo (100) tunnel barriers, Nature materials **3**, 862 (2004).

[9] A. Brataas, A. D. Kent, and H. Ohno, Current-induced torques in magnetic materials, Nature materials **11**, 372 (2012).

[10] A. Brataas, A. D. Kent, and H. Ohno, Current-induced torques in magnetic materials, Nature materials **11**, 372 (2012).

[11] K. Ando, S. Fujita, J. Ito, S. Yuasa, Y. Suzuki, Y. Nakatani, T. Miyazaki, and H. Yoda, Spin-transfer torque magnetoresistive random-access memory technologies for normally off computing, Journal of Applied Physics **115**, 172607 (2014).

[12] A. Khvalkovskiy, D. Apalkov, S. Watts, R. Chepulskii, R. Beach, A. Ong, X. Tang, A. Driskill-Smith, W. Butler, P. Visscher, *et al.*, Basic principles of stt-mram cell operation in memory arrays, Journal of Physics D: Applied Physics **46**, 074001 (2013).

[13] A. Manchon, J. Železnỳ, I. M. Miron, T. Jungwirth, J. Sinova, A. Thiaville, K. Garello, and P. Gambardella, Current-induced spin-orbit torques in ferromagnetic and antiferromagnetic systems, Reviews of Modern Physics **91**, 035004 (2019).

[14] I. M. Miron, K. Garello, G. Gaudin, P.-J. Zermatten, M. V. Costache, S. Auffret, S. Bandiera, B. Rodmacq, A. Schuhl, and P. Gambardella, Perpendicular switching of a single ferromagnetic layer induced by in-plane current injection, Nature **476**, 189 (2011).

[15] V. Krizakova, M. Perumkunnil, S. Couet, P. Gambardella, and K. Garello, Spin-orbit torque switching of magnetic tunnel junctions for memory applications, Journal of Magnetism and Magnetic Materials **562**, 169692 (2022).

[16] C. D. Stanciu, F. Hansteen, A. V. Kimel, A. Kirilyuk, A. Tsukamoto, A. Itoh, and T. Rasing, All-optical magnetic recording with circularly polarized light, Physical review letters **99**, 047601 (2007).

[17] I. Radu, K. Vahaplar, C. Stamm, T. Kachel, N. Pontius, H. Dürr, T. Ostler, J. Barker, R. Evans, R. Chantrell, *et al.*, Transient ferromagnetic-like state mediating ultrafast reversal of antiferromagnetically coupled spins, Nature **472**, 205 (2011).

[18] T. Ostler, J. Barker, R. Evans, R. Chantrell, U. Atxitia, O. Chubykalo-Fesenko, S. El Moussaoui, L. Le Guyader, E. Mengotti, L. Heyderman, *et al.*, Ultrafast heating as a sufficient stimulus for magnetization reversal in a ferrimagnet, Nature communications **3**, 666 (2012).

[19] E. Y. Vedmedenko, R. K. Kawakami, D. D. Sheka, P. Gambardella, A. Kirilyuk, A. Hirohata, C. Binek, O. Chubykalo-Fesenko, S. Sanvito, B. J. Kirby, *et al.*, The 2020 magnetism roadmap, Journal of Physics D: Applied Physics **53**, 453001 (2020).

[20] L. Avilés-Félix, L. Álvaro-Gómez, G. Li, C. Davies, A. Olivier, M. Rubio-Roy, S. Auffret, A. Kirilyuk, A. Kimel, T. Rasing, *et al.*, Integration of tb/co multilayers within optically switchable perpendicular magnetic tunnel junctions, Aip Advances **9**, 125328 (2019).

[21] L. Avilés-Félix, A. Olivier, G. Li, C. S. Davies, L. Álvaro-Gómez, M. Rubio-Roy, S. Auffret, A. Kirilyuk, A. Kimel, T. Rasing, *et al.*, Single-shot all-optical switching of magnetization in tb/co multilayer-based electrodes, Scientific reports **10**, 5211 (2020).

[22] K. Mishra, T. G. H. Blank, C. S. Davies, L. Avilés-Félix, D. Salomoni, L. D. Buda-Prejbeanu, R. C. Sousa, I. L. Prejbeanu, B. Koopmans, T. Rasing, A. V. Kimel, and A. Kirilyuk, Dynamics of all-optical single-shot switching of magnetization in tb/co multilayers, Phys. Rev. Res. **5**, 023163 (2023).

[23] Y. Peng, D. Salomoni, G. Malinowski, W. Zhang, J. Hohlfeld, L. Buda-Prejbeanu, J. Gorchon, M. Vergès, J. Lin, R. Sousa, *et al.*, In plane reorientation induced single laser pulse magnetization reversal in rare-earth based multilayer, arXiv preprint arXiv:2212.13279 (2022).

[24] J. Igarashi, W. Zhang, Q. Remy, E. Díaz, J.-X. Lin, J. Hohlfeld, M. Hehn, S. Mangin, J. Gorchon, and G. Malinowski, Optically induced ultrafast magnetization switching in ferromagnetic spin valves, Nature Materials , 1 (2023).

[25] J.-Y. Chen, L. He, J.-P. Wang, and M. Li, All-optical switching of magnetic tunnel junctions with single subpicosecond laser pulses, Physical Review Applied **7**, 021001 (2017).

[26] L. Wang, H. Cheng, P. Li, Y. L. van Hees, Y. Liu, K. Cao, R. Lavrijsen, X. Lin, B. Koopmans, and W. Zhao, Pi-

cosecond optospintronic tunnel junctions, Proceedings of the National Academy of Sciences **119**, e2204732119 (2022).

[27] S. Mondal, D. Polley, A. Pattabi, J. Chatterjee, D. Salomoni, L. Aviles-Felix, A. Olivier, M. Rubio-Roy, B. Diény, L. D. B. Prejbeanu, R. Sousa, I. L. Prejbeanu, and J. Bokor, Single-shot switching in tb/co-multilayer based nanoscale magnetic tunnel junctions, Journal of Magnetism and Magnetic Materials **581**, 170960 (2023).

[28] F. Dumas-Bouchiat, H. Nagaraja, F. Rossignol, C. Champeaux, G. Trolliard, A. Catherinot, and D. Givord, Cobalt cluster-assembled thin films deposited by low energy cluster beam deposition: Structural and magnetic investigations of deposited layers, Journal of applied physics **100** (2006).

[29] F. Darnell, Lattice parameters of terbium and erbium at low temperatures, Physical Review **132**, 1098 (1963).

[30] J. Yue, S. Jiang, D. Zhang, H. Yuan, Y. Wang, L. Lin, Y. Zhai, J. Du, and H. Zhai, The influence of interface on spin pumping effect in ni80fe20/tb bilayer, AIP Advances **6** (2016).

[31] A. Rebei and J. Hohlfeld, Origin of increase of damping in transition metals with rare-earth-metal impurities, Physical review letters **97**, 117601 (2006).

[32] G.-M. Choi, B.-C. Min, K.-J. Lee, and D. G. Cahill, Spin current generated by thermally driven ultrafast demagnetization, Nature communications **5**, 4334 (2014).

[33] E. Beaurepaire, J.-C. Merle, A. Daunois, and J.-Y. Bigot, Ultrafast spin dynamics in ferromagnetic nickel, Physical review letters **76**, 4250 (1996).

[34] L. Avilés-Félix, L. Farcis, Z. Jin, L. Álvaro-Gómez, G. Li, K. T. Yamada, A. Kirilyuk, A. V. Kimel, T. Rasing, B. Dieny, *et al.*, All-optical spin switching probability in [tb/co] multilayers, Scientific Reports **11**, 6576 (2021).

[35] D. S. Hazen, S. Auffret, I. Joumard, L. Vila, L. D. Buda-Prejbeanu, R. C. Sousa, L. Prejbeanu, and B. Dieny, Double magnetic tunnel junctions with a switchable assistance layer for improved spin transfer torque magnetic memory performance, Nanoscale **13**, 14096 (2021).

[36] L. Ertl, G. Endl, and H. Hoffmann, Structure and magnetic properties of sputtered tb/co multilayers, Journal of magnetism and magnetic materials **113**, 227 (1992).

[37] W. Thoburn, S. Legvold, and F. Spedding, Magnetic properties of terbium metal, Physical Review **112**, 56 (1958).

[38] J. Coey, Amorphous magnetic order, Journal of Applied Physics **49**, 1646 (1978).

[39] A. Olivier, L. Avilés-Félix, A. Chavent, L. Álvaro-Goémez, M. Rubio-Roy, S. Auffret, L. Vila, B. Dieny, R. C. Sousa, and I. Prejbeanu, Indium tin oxide optical access for magnetic tunnel junctions in hybrid spintronic–photonic circuits, Nanotechnology **31**, 425302 (2020).

[40] E. K. Sobolewska, J. Pelloux-Prayer, H. Becker, G. Li, C. S. Davies, C. Krückel, L. A. Félix, A. Olivier, R. C. Sousa, I.-L. Prejbeanu, *et al.*, Integration platform for optical switching of magnetic elements, in *Active Photonic Platforms XII*, Vol. 11461 (SPIE, 2020) pp. 54–72.

[41] A. Hylick, R. Sohan, A. Rice, and B. Jones, An analysis of hard drive energy consumption, in *2008 IEEE International Symposium on Modeling, Analysis and Simulation of Computers and Telecommunication Systems* (IEEE, 2008) pp. 1–10.

[42] J. P. Liu, E. Fullerton, O. Gutfleisch, and D. J. Sellmyer, *Nanoscale magnetic materials and applications* (Springer, 2009).

[43] K. Wang, J. Alzate, and P. K. Amiri, Low-power non-volatile spintronic memory: Stt-ram and beyond, Journal of Physics D: Applied Physics **46**, 074003 (2013).

[44] W. Zhang, J. X. Lin, T. X. Huang, G. Malinowski, M. Hehn, Y. Xu, S. Mangin, and W. Zhao, Role of spin-lattice coupling in ultrafast demagnetization and all optical helicity-independent single-shot switching in gd 1-x- y tb y co x alloys, Physical Review B **105**, 054410 (2022).

[45] G. Kichin, M. Hehn, J. Gorchon, G. Malinowski, J. Hohlfeld, and S. Mangin, From multiple-to single-pulse all-optical helicity-dependent switching in ferromagnetic co/pt multilayers, Physical Review Applied **12**, 024019 (2019).

[46] C. Davies, K. Prabhakara, M. Davydova, K. Zvezdin, T. Shapaeva, S. Wang, A. Zvezdin, A. Kirilyuk, T. Rasing, and A. Kimel, Anomalously damped heat-assisted route for precessional magnetization reversal in an iron garnet, Physical review letters **122**, 027202 (2019).

[47] L. Shelukhin, V. Pavlov, P. Usachev, P. Y. Shamray, R. Pisarev, and A. Kalashnikova, Ultrafast laser-induced changes of the magnetic anisotropy in a low-symmetry iron garnet film, Physical Review B **97**, 014422 (2018).

[48] Q. Remy, J. Igarashi, S. Iihama, G. Malinowski, M. Hehn, J. Gorchon, J. Hohlfeld, S. Fukami, H. Ohno, and S. Mangin, Energy efficient control of ultrafast spin current to induce single femtosecond pulse switching of a ferromagnet, Advanced Science **7**, 2001996 (2020).

[49] J. Igarashi, Q. Remy, S. Iihama, G. Malinowski, M. Hehn, J. Gorchon, J. Hohlfeld, S. Fukami, H. Ohno, and S. Mangin, Engineering single-shot all-optical switching of ferromagnetic materials, Nano Letters **20**, 8654 (2020).

[50] A. Drovosekov, D. Kholin, and N. Kreinies, Magnetic properties of layered ferrimagnetic structures based on gd and transition 3 d metals, Journal of Experimental and Theoretical Physics **131**, 149 (2020).